sample (100 μL) of the catalysis solution was diluted with benzene (500 μL) and the precipitated catalyst was filtered off. Azeotropic distillation yielded a viscous oil, which was examined by ^{1}H NMR spectroscopy. All of the four possible cyclization products were observed in C_6D_6, and the major product (80%) was confirmed to be *l*-isopulegol by a ^{1}H NMR comparison with the reported spectrum.[11]

Crystal Structure. Preliminary photographic characterization revealed no symmetry higher than triclinic; this was later confirmed by TRACER. The centrosymmetric space group alternative was initially chosen statistically. The chemically reasonable bond parameters obtained from refinement suggested that this assignment was correct. A linear correlation for a 30% decay in the check reflection intensity during data collection (due to loss of acetone) and an empirical absorption correction were applied to the data.

An autointerpreted Patterson routine was used to locate the Ru and Sb atoms. All non-hydrogen atoms were refined anisotropically, and hydrogen atoms were treated as idealized, isotropic contributions. All computations used SHELXTL (version 5.1) software (G. Sheldrick, Nicolet (Siemens), Madison, WI).

Acknowledgment. This work was supported by grants from the National Institutes of Health.

Supplementary Material Available: Tables of bond distances, bond angles, atomic coordinates, and anisotropic/isotropic thermal parameters (7 pages); a listing of structure factors (13 pages). Ordering information is given on any current masthead page.

Ground Spin State Variability in Manganese Oxo Aggregates. Demonstration of an $S = {}^3/_2$ Ground State for $[Mn_3O_4(OH)(bpea)_3](ClO_4)_3$[1]

Samudranil Pal, Michael K. Chan, and William H. Armstrong*,†

Contribution from the Department of Chemistry, University of California, Berkeley, California 94720. *Received December 30, 1991*

Abstract: Synthesis and properties of bi- and trinuclear manganese oxo complexes of the ligand *N,N*-bis(2-pyridylmethyl)ethylamine (bpea) are reported. The binuclear species $[Mn_2O_2(O_2CCH_3)(bpea)_2](ClO_4)_3$ (**1**) was isolated in 41% yield from a MeOH reaction mixture that contained $Mn(O_2CCH_3)_3{\cdot}2H_2O$, bpea, and aqueous $HClO_4$. Compound **1** crystallizes from $CHCl_3$/CH_3CN/*n*-hexane as **1**·CH_3CN·0.5$CHCl_3$ in the triclinic space group $P\bar{1}$ with a = 12.956 (1) Å, b = 12.987 (2) Å, c = 13.391 (2) Å, α = 77.20 (1)°, β = 83.34 (1)°, γ = 80.36 (1)°, V = 2158.8 (6) Å^3, and Z = 2. Bond distances and angles for **1** are consistent with a Mn^{IV}_2 oxidation state assignment. The variable temperature magnetic susceptibility data for **1** in the range 6–280 K were fit with the expression generated from the isotropic spin Hamiltonian $\mathcal{H} = -2J\hat{S}_1{\cdot}\hat{S}_2$ ($S_1 = S_2 = {}^3/_2$), with J = −124 cm^{-1}. Compound **1** was converted to $[Mn_3O_4(OH)(bpea)_3](ClO_4)_3$ (**2**) in 90% yield by adding an aqueous solution of $NaClO_4$ to a CH_3CN solution of **1**. Compound **2** crystallizes from $CH_3CN/C_6H_5CH_3$ in the monoclinic space group $P2_1/n$ with a = 10.875 (4) Å, b = 26.074 (9) Å, c = 18.437 (5) Å, β = 103.80 (2)°, V = 5077.2 (6) Å^3, and Z = 4. The structure of **2** consists of three Mn(IV) ions, with two (Mn_b) being coupled together by two doubly-bridging oxo groups (O_b) and the third (Mn_a) being singly-bridged to each Mn_b atom by oxo groups (O_a). Atom Mn_a bears a terminal OH group which is hydrogen bonded to an O_b group. This interaction appears to be in part responsible for a distortion that brings Mn_a out of the plane of the two Mn_b and two O_a atoms. The EPR spectral properties of **2** are consistent with an $S = {}^3/_2$ ground state. Magnetic susceptibility data in the range 6–280 K using an applied magnetic field of 5 kG were also consistent with an $S = {}^3/_2$ ground state and were fit using the Hamiltonian $\mathcal{H} = -2J(\hat{S}_1{\cdot}\hat{S}_2) - 2J'(\hat{S}_1{\cdot}\hat{S}_3 + \hat{S}_2{\cdot}\hat{S}_3)$ ($S_1 = S_2 = S_3 = {}^3/_2$; J = −76 cm^{-1}, J' = −11 cm^{-1}). Both **1** and **2** were further characterized with UV–vis, infrared, and electrochemical measurements. The relationship between **2** and two other species that contain the $\{Mn_3O_4\}^{4+}$ core is discussed. The similarity between the ground spin state variability for synthetic trinuclear manganese oxo complexes and the manganese site in photosystem II is noted.

Introduction

Currently, an abundance of experimental evidence suggests that water oxidation and accompanying dioxygen generation take place in photosynthetic organisms at a polynuclear manganese aggregate within the thylakoid membrane-bound photosystem II oxygen-evolving complex (MnOEC).[2-4] The exact nature of this manganese complex has not been established despite the fact that it has been characterized extensively with a variety of spectroscopic and magnetic techniques.[2,3] X-ray absorption experiments have established the existence of at least two 2.7-Å Mn···Mn contacts within the MnOEC. Attempts to prepare synthetic analogs for the MnOEC have led to the discovery of many interesting polynuclear manganese–oxo species.[5-11] To our knowledge only one of these, $[(Mn_2O_2)_2(tphpn)_2]^{4+}$,[12] faithfully mimics an EPR signal associated with the MnOEC.

A fascinating feature of the PSII manganese aggregate when poised at the so-called Kok S_2 oxidation level is the existence of two distinctly different EPR spectral signatures:[2,3] (i) a signal centered at g = 2 with a minimum of 16 hyperfine components at X-band frequency and (ii) a broad absorption with g_{eff} = 4.1

† Current address: Department of Chemistry, Boston College, Chestnut Hill, MA 02167.

(1) Abbreviations used are as follows: PSII, photosystem II; OEC, oxygen evolving complex; EXAFS, extended X-ray absorption fine structure; EPR, electron paramagnetic resonance; NMR, nuclear magnetic resonance; IR, infrared; bpea, *N,N*-bis(2-pyridylmethyl)ethylamine; tmtacn, *N,N',N''*-trimethyl-1,4,7-triazacyclononane; tacn, 1,4,7-triazacyclononane; $HBpz_3$, hydrotris(pyrazol-1-yl)borate; phen, 1,10-phenanthroline; bpy, 2,2'-bipyridine; tpma, tris(2-pyridylmethyl)amine; pic, picolinic acid; bispicen, *N,N'*-bis(2-pyridylmethyl)-1,2-ethanediamine; tpen, *N,N,N',N'*-tetrakis(2-pyridylmethyl)-1,2-ethanediamine; dmepa, ((6-methyl-2-pyridyl)methyl)(2-(2-pyridylethyl))(2-pyridylmethyl)amine; salpn, 1,3-bis((2-hydroxybenzyl)imino)propane; 5-NO_2-sadpen, bis(3-((2-hydroxy-5-nitrobenzyl)imino)propyl)-methylamine; bispictn, *N,N'*-bis(2-pyridylmethyl)-1,3-propanediamine; bispicbn, *N,N'*-bis(2-pyridylmethyl)-2,3-butanediamine; bispichxn, *N,N'*-bis(2-pyridylmethyl)-1,2-cyclohexanediamine; Fc, ferrocene; TEAP, tetraethylammonium percholorate.

(2) Debus, R. J. *Biochim. Biophys. Acta* (*Reviews in Bioenergetics*), in press.

(3) Brudvig, G. W.; Beck, W. F.; dePaula, J. C. *Annu. Rev. Biophys. Chem.* **1989**, *18*, 25–46.

(4) Govindjee; Coleman, W. *Sci. Am.* **1990**, *262*, 50–58.

(5) Armstrong, W. H. In *Bioinorganic Chemistry of Manganese*; Pecoraro, V. L., Ed.; VCH: New York, 1992; pp 261–286.

0002-7863/92/1514-6398$03.00/0

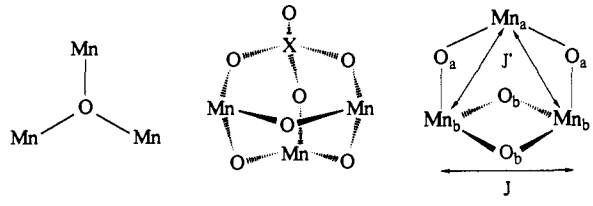

Figure 1. Trinuclear manganese oxo structural types. Magnetic exchange scheme for the $\{Mn_3O_4\}^{4+}$ core is shown at the far right.

on which at least 16 hyperfine lines were recently detected by Kim et al.[13] using oriented samples. The relative intensities of the $g = 2$ and $g = 4.1$ EPR signals vary as a function of conditions, including the cryoprotectants used for freezing samples. A plausible explanation that has been put forth to account for the two EPR signals is that two conformations of the polynuclear Mn aggregate are readily accessible, one which has an $S = {}^1/_2$ spin ground state ("multiline conformation") and the other with a ground state of $S \geq {}^3/_2$ ("$g = 4.1$ conformation").[8]

It is interesting to note that another tetranuclear aggregate which plays an important role in biology, namely, $\{Fe_4S_4\}^+$, exhibits variable ground spin state behavior.[14-17] This sulfide-bridged cluster, found in various ferredoxins, is generally observed to be in a conformation which gives rise to a ground spin state of $S = {}^1/_2$. On the other hand, the $\{Fe_4S_4\}^+$ aggregate in the molybdenum[14-16] and vanadium[17] nitrogenase Fe proteins exhibits both $S = {}^1/_2$ and $S = {}^3/_2$ ground states, depending on solvent and exogenous ligand binding conditions. Holm and co-workers have observed the same sort of phenomenon for their ferredoxin synthetic analogs.[18,19] Although the synthetic analog complexes $[Fe_4S_4(SR)_4]^{3-}$ predominantly display $S = {}^1/_2$ ground states in solution, crystal packing induces subtle conformational changes such that higher spin ground states have been observed in the solid state. A recent report[19] from Holm's laboratory on this subject concluded that there was no distinct correlation between any structural parameter of the $\{Fe_4S_4\}^+$ core or of the terminal ligand conformation and the observed ground spin state.

It is reasonable to expect that there are at least three magnetically coupled manganese ions in the MnOEC aggregate that displays ground spin state variability. This hypothesis is based on the many observations of well-separated $S = {}^1/_2$ ground states for $\{Mn_2O_2\}^{3+}$ complexes as a result of strong intramolecular antiferromagnetic interactions.[20-26] It is difficult to imagine that an energetically reasonable conformational change in the $\{Mn_2O_2\}$ core could induce a ground spin state change. Addition of a third manganese ion dramatically changes the situation with regard to accessible electronic structures (see below). One might argue that a dimeric substructure of the MnOEC could show ground spin state variability if there were a weak magnetic interaction between Mn atoms. For example, two compounds that contain the magnetically weakly coupled $\{Mn^{III}_2O(O_2CCH_3)_2\}^{2+}$ core, $[Mn_2O(O_2CCH_3)_2(bpy)_2Cl_2]$[27] and $[Mn_2O(O_2CCH_3)_2(tmtacn)_2]^{2+}$,[28] exhibit low-spin and high-spin ground states, respectively, corresponding to an antiferromagnetic interaction ($J = -4$ cm^{-1})[27] for the former and a ferromagnetic interaction ($J = +9$ cm^{-1})[28] for the latter. For a third species, $[Mn_2O(O_2CCH_3)_2(HBpz_3)_2]$, there is almost no interaction between manganese ions ($J = -0.2$ to -0.7 cm^{-1}).[29,30] However, it is unlikely that an *isolated* $\{Mn_2O(O_2CCH_3)_2\}$ substructure exists within the MnOEC as EXAFS measurements indicate at least two ~2.7-Å Mn···Mn contacts to be present therein.

Three types of trinuclear manganese oxo compounds have been reported to date, those containing the $\{Mn_3(\mu_3\text{-}O)\}$,[31-34] $\{Mn^{IV}_3(\mu\text{-}O)_3(\mu\text{-}XO_4)\}$ (X = P, As, or V),[35] and $\{Mn^{IV}_3(\mu\text{-}O)_4\}$[36,37] core types (Figure 1). None of these have obvious direct relevance to the MnOEC. Wieghardt et al. demonstrated that $[Mn_3O_3(PO_4)(tacn)_3]^{3+}$ has a ground spin state of $S = {}^1/_2$.[35] Both $[Mn_3O_4Cl_2(bpy)_4]^{2+}$ [36] and $[Mn_3O_4(H_2O)_2(bpy)_4]^{4+}$ [37] have variable temperature magnetic susceptibility behavior consistent with that expected for $S = {}^1/_2$ ground states, and both exhibit 35-line EPR signals at X-band frequencies. These multiline signals are quite distinct from the multiline signal observed for the MnOEC mentioned above, although all three arise from $S = {}^1/_2$ electronic states. In the course of our ongoing investigation of the higher valent manganese coordination chemistry of the facially binding tridentate ligand *N,N*-bis(2-pyridylmethyl)ethylamine (bpea), we have isolated bi- and trinuclear manganese–oxo complexes: $[Mn_2O_2(O_2CCH_3)(bpea)_2](ClO_4)_3$ (**1**) and $[Mn_3O_4(OH)(bpea)_3](ClO_4)_3$ (**2**). Compound **2** represents the third example of the $\{Mn_3O_4\}^{4+}$ core. Interestingly, its electronic properties are quite distinct from those of the bpy species mentioned above. In this report we describe the synthesis, structure, and magnetic properties of the binuclear and trinuclear bpea species. Of particular interest is the contrast between the ground spin state properties of **2** and $[Mn_3O_4X_2(bpy)_4]^{n+}$ (X = Cl, $n = 2$, **3**; X = H_2O, $n = 4$, **4**). The relationship between the spin-state properties of the synthetic trinuclear aggregates and the proposed spin-state variability of the photosystem II manganese site is also of concern.

Experimental Section

Materials. 2-Picolyl chloride hydrochloride and manganese(III) acetate dihydrate were purchased from Aldrich Chemical Co. An aqueous solution of ethylamine (70%) was obtained from Eastman Kodak

(6) Pecoraro, V. L. *Photochem. Photobiol.* **1988**, *48*, 249–264.
(7) Wieghardt, K. *Angew. Chem., Int. Ed. Engl.* **1989**, *28*, 1153–1172.
(8) Brudvig, G. W.; Crabtree, R. H. *Prog. Inorg. Chem.* **1989**, *37*, 99–142.
(9) Thorp, H. H.; Brudvig, G. W. *New. J. Chem.* **1991**, *15*, 479–490.
(10) Brudvig, G. W.; Thorp, H. H.; Crabtree, R. H. *Acc. Chem. Res.* **1991**, *24*, 311–316.
(11) Christou, G. *Acc. Chem. Res.* **1989**, *22*, 328–335.
(12) Chan, M. K.; Armstrong, W. H. *J. Am. Chem. Soc.* **1991**, *113*, 5055–5057.
(13) Kim, D. H.; Britt, R. D.; Klein, M. P.; Sauer, K. *J. Am. Chem. Soc.* **1990**, *112*, 9389–9391.
(14) Lindahl, P. A.; Day, E. P.; Kent, T. A.; Orme-Johnson, W. H.; Munck, E. *J. Biol. Chem.* **1985**, *260*, 11160–11173.
(15) Meyer, J.; Gaillard, J.; Moulis, J.-M. *Biochemistry* **1988**, *27*, 6150–6156.
(16) Lindahl, P. A.; Gorelick, N. J.; Munck, E.; Orme-Johnson, W. H. *J. Biol. Chem.* **1987**, *262*, 14945–14953.
(17) Hales, B. J.; Langosch, D. J.; Case, E. E. *J. Biol. Chem.* **1986**, *261*, 15301–15306.
(18) Carney, M. J.; Papaefthymiou, G. C.; Frankel, R. B.; Holm, R. H. *Inorg. Chem.* **1989**, *28*, 1497–1503.
(19) Carney, M. J.; Papaefthymiou, G. C.; Spartalian, K.; Frankel, R. B.; Holm, R. H. *J. Am. Chem. Soc.* **1988**, *110*, 6084–6095.
(20) Cooper, S. R.; Dismukes, G. C.; Klein, M. P.; Calvin, M. *J. Am. Chem. Soc.* **1978**, *100*, 7248–7252.
(21) Hagen, K. S.; Armstrong, W. H.; Hope, H. *Inorg. Chem.* **1988**, *27*, 967–969.
(22) Stebler, M.; Ludi, A.; Bürgi, H.-B. *Inorg. Chem.* **1986**, *25*, 4743–4750.
(23) Collins, M. A.; Hodgson, D. J.; Michelsen, K.; Towle, D. K. *J. Chem. Soc., Chem. Commun.* **1987**, 1659–1660.
(24) Suzuki, M.; Senda, H.; Kobayashi, Y.; Oshio, H.; Uehara, A. *Chem. Lett.* **1988**, 1763–1766.
(25) Suzuki, M.; Tokura, S.; Suhara, M.; Uehara, A. *Chem. Lett.* **1988**, 477–480.
(26) Towle, D. K.; Botsford, C. A.; Hodgson, D. J. *Inorg. Chim. Acta* **1988**, *141*, 167–168.
(27) Menage, S.; Girerd, J. J.; Gleizes, A. *J. Chem. Soc., Chem. Commun.* **1988**, 431–432.
(28) Wieghardt, K.; Bossek, U.; Ventur, D. J.; Weiss, J. *J. Chem. Soc., Chem. Commun.* **1985**, 347–349.
(29) Sheats, J. E.; Czernuszewicz, R. S.; Dismukes, G. C.; Rheingold, A. L.; Petrouleas, V.; Stubbe, J.; Armstrong, W. H.; Beer, R. H.; Lippard, S. J. *J. Am. Chem. Soc.* **1987**, *109*, 1435–1444.
(30) The magnetic exchange coupling constants quoted correspond to a Hamiltonian of the form $\mathcal{H} = -2JS_1 \cdot S_2$.
(31) Baikie, A. R. E.; Hursthouse, M. B.; New, D. B.; Thornton, P. *J. Chem. Soc., Chem. Commun.* **1978**, 62–63.
(32) Baikie, A. R. E.; Hursthouse, M. B.; New, L.; Thornton, P.; White, R. G. *J. Chem. Soc., Chem. Commun.* **1980**, 684–685.
(33) Lis, T.; Jezowska-Trzebiatowska, B. *Acta Crystallogr.* **1977**, *B33*, 2112–2116.
(34) Vincent, J. B.; Chang, H.-R.; Folting, K.; Huffman, J. C.; Christou, G.; Hendrickson, D. N. *J. Am. Chem. Soc.* **1987**, *109*, 5703–5711.
(35) Wieghardt, K.; Bossek, U.; Nuber, B.; Weiss, J.; Gehring, S.; Haase, W. *J. Chem. Soc., Chem. Commun.* **1988**, 1145–1146.
(36) Auger, N.; Girerd, J.-J.; Corbella, M.; Gleizes, A.; Zimmermann, J.-L. *J. Am. Chem. Soc.* **1990**, *112*, 448–450.
(37) Sarneski, J. E.; Thorp, H. H.; Brudvig, G. W.; Crabtree, R. H.; Schulte, G. K. *J. Am. Chem. Soc.* **1990**, *112*, 7255–7260.

Co. Acetonitrile used for electrochemical experiments was purified by distillation from CaH_2 and stored over 3-Å molecular sieves. The supporting electrolyte tetraethylammonium perchlorate (TEAP) was prepared by following a reported procedure.[38] All other solvents and chemicals were analytical grade and used as supplied.

Physical Measurements. IR spectra were collected by using KBr pellets on a Nicolet 5DX Fourier transform infrared spectrometer. Electronic spectra were recorded by using a Perkin-Elmer Lambda 9 UV/vis/near-IR spectrophotometer. The ^1H NMR spectrum was taken on a 250-MHz Fourier transform spectrometer, equipped with a Cryomagnets, Inc. magnet and a Nicolet Model 1280 data collection system. The EPR spectrum was obtained by using an IBM 2090D-SRC spectrometer fitted with a quartz dewar for low-temperature measurements (liquid dinitrogen, 77 K) or a Varian E-109 spectrometer (at 6 K) equipped with an Air Products Model LTR liquid helium cryostat. Solid-state magnetic susceptibility measurements were performed on a Model 800 VTS-50 SQUID magnetometer (S.H.E. Corporation) in the temperature range 6–280 K. All data were corrected for the susceptibility of the empty sample container. Diamagnetic corrections (-474×10^{-6} and -642×10^{-6} cgsu for **1** and **2**, respectively) calculated from Pascal's constants[39] were used to obtain the molar paramagnetic susceptibilities. Electrochemical experiments were performed with an EG&G PAR Model 264A polarographic analyzer/stripping voltameter linked with a locally constructed Supercycle triangle wave generator.[40] A platinum disk working electrode, a platinum wire auxiliary electrode, and a saturated sodium calomel reference electrode (SSCE) were used for the electrochemical measurements. All electrochemical experiments were carried out under a dry and purified dinitrogen atmosphere. In acetonitrile under the identical conditions as used for **1** and **2**, the $E_{1/2}$ of the Fc/Fc^+ couple was +0.39 V (ΔE_p = 80 mV). The potentials reported in this work are uncorrected for junction contributions. Elemental analyses were obtained from the University of California, Berkeley Microanalytical Laboratory.

Preparation of Compounds. A. *N,N*-Bis(2-pyridylmethyl)ethylamine (bpea). To an aqueous solution (40 mL) of 2-picolyl chloride hydrochloride (8.2 g, 0.05 mol) was added 1.61 mL of an aqueous solution (70%) of ethylamine (1.127 g, 0.025 mol). The mixture was stirred and heated to 60 °C. To this solution was added over a period of 1 h 10 mL of an aqueous solution of NaOH (4 g, 0.1 mol). The dark brown mixture was stirred for an additional $^1/_2$ h and then cooled to room temperature. The mixture was extracted with chloroform, and the deep brown extract was concentrated by rotary evaporation to a thick oil. The oil was dissolved in 10 mL of chloroform, the solution was absorbed on basic alumina (80–200 mesh) and finally eluted with chloroform, and the light yellow solution was evaporated. A yellow oil was obtained as the final product. This procedure provided 5 g (88% yield) of bpea that was of sufficient purity for use in the manganese coordination chemistry that follows. ^1H NMR (250 MHz) ($CDCl_3$, Me_4Si reference)[41] (δ, ppm (J, Hz) (multiplicity)): ethyl CH_3, 1.11 (7.1) (t); ethyl CH_2, 2.64 (7.1) (q); pyridylmethyl CH_2, 3.82 (s); pyridine hydrogen atoms, 7.11 (6.0) (t), 7.54 (7.7) (d), 7.63 (7.6) (t), 8.51 (3.6) (d).

B. $[Mn_2O_2(O_2CCH_3)(bpea)_2](ClO_4)_3$ (1). To a methanol solution (25 mL) of bpea (454 mg, 2 mmol) was added solid $Mn(O_2CCH_3)_3 \cdot 2H_2O$ (536 mg, 2 mmol). The mixture was stirred in air at room temperature for 15 min and then filtered. To the red-brown filtrate was added 0.60 mL of 70% aqueous perchloric acid, and the mixture was stirred for an additional 1 h. The brown precipitate that appeared was collected by filtration, washed thoroughly with methanol, and finally dried in vacuum. The yield of **1** was 350 mg (41%). Anal. Calcd for $Mn_2C_{30}H_{37}N_6O_{16}Cl_3$: Mn, 11.52; C, 37.77; H, 3.91; N, 8.81. Found: Mn, 11.4; C, 37.28; H, 3.87; N, 8.20. Selected IR bands[42] (cm^{-1}): 1610 (s), 1571 (s), 1560 (s), 1487 (s), 1437 (s), 1387 (s), 1337 (m), 1308 (w), 1290 (m), 1144 (sh), 1091 (vs), 1056 (sh), 1035 (m), 997 (w), 769 (s), 693 (m), 669 (s), 637 (m), 622 (s). Electronic spectral data in CH_3CN solution (λ_{max}, nm (ϵ, M^{-1} cm^{-1})): 820 (sh), 630 (sh), 580 (sh), 454 (2180).

C. $[Mn_3O_4(OH)(bpea)_3](ClO_4)_3$ (2). To a red-brown acetonitrile solution (20 mL) of **1** (400 mg, 0.42 mmol) was added 100 mL of distilled water, and the solution was stirred in air at room temperature for 1.5 h. An aqueous solution (20 mL) of $NaClO_4 \cdot H_2O$ (4 g, 0.028 mol) was added, and the mixture was stirred for another 3.5 h. The red-brown microcrystalline solid that had deposited was collected by filtration (filtrate pH ≈ 4), washed with methanol, and dried in vacuum. This procedure afforded 310 mg (90% yield) of **2**. Anal. Calcd for $Mn_3C_{42}H_{52}N_9O_{17}Cl_3$: Mn, 13.44; C, 41.14; H, 4.27; N, 10.28. Found: Mn, 13.3; C, 41.04; H, 4.12; N, 9.97. Selected IR bands[42] (cm^{-1}): 1607 (s), 1574 (m), 1486 (s), 1437 (s), 1393 (m), 1305 (w), 1287 (m), 1161 (m), 1091 (vs), 1056 (sh), 1032 (m), 997 (w), 880 (w), 772 (s), 695 (m), 672 (s), 657 (w), 637 (w), 622 (s). Electronic spectral data in CH_3CN solution (λ_{max}, nm (ϵ, M^{-1} cm^{-1})): 767 (190), 600 (sh), 490 (sh), 370 (sh).

Table I. Crystallographic Data for $[Mn_2O_2(O_2CCH_3)(bpea)_2](ClO_4)_3 \cdot CH_3CN \cdot 0.5CHCl_3$ ($1 \cdot CH_3CN \cdot 0.5CHCl_3$) and $[Mn_3O_4(OH)(bpea)_3](ClO_4)_3$ (**2**)

	$1 \cdot CH_3CN \cdot 0.5CHCl_3$	**2**
chemical formula	$Mn_2Cl_{4.5}O_{16}N_7C_{32.5}H_{40.5}$	$Mn_3Cl_3O_{17}N_9C_{42}H_{52}$
formula weight	1054.635	1226.11
temp, K	202	204
space group	$P\bar{1}$	$P2_1/n$
a, Å	12.9563 (12)	10.875 (4)
b, Å	12.9868 (22)	26.074 (9)
c, Å	13.3906 (20)	18.437 (5)
α, deg	77.198 (13)	90
β, deg	83.337 (9)	103.80 (2)
γ, deg	80.360 (11)	90
V, Å^3	2158.8 (6)	5077.2 (6)
Z	2	4
d_{calcd}, g cm^{-3}	1.622	1.604
μ, cm^{-1}	9.157	9.405
diffractometer	Enraf-Nonius CAD-4	
radiation	Mo Kα	
λ, Å	0.71073	
monochromator	graphite	
crystal size, mm	0.31 × 0.24 × 0.22	0.32 × 0.62 × 0.41
octants collected	$h,\pm k,\pm l$	$h,k,\pm l$
max hkl	13,14,14	11,28,19
2θ range, deg	3–45	3–45
collection method	θ–2θ	ω–2θ
data collected	5622	6617
data used ($I > 3\sigma(I)$)	3694	4719
no. of variables	545	660
R,[a] %	4.87	4.97
R_w,[b] %	5.42	5.84
max, min peak on final diff Fourier map, e/Å^3	0.62, −0.11	1.22, −0.12
GOF[c]	1.772	2.255

[a] $R = (\sum||F_o| - |F_c||)/\sum|F_o|$. [b] $R_w = \{[\sum w(|F_o| - |F_c|)^2]/\sum wF_o^2\}^{1/2}$. [c] GOF = $\{[\sum w(|F_o| - |F_c|)^2]/(n_o - n_v)\}^{1/2}$; $w = 4F_o^2/[\sigma(I)^2 + (pF_o^2)^2]$, where $p = 0.03$.

X-ray Crystallography. A. $[Mn_2O_2(O_2CCH_3)(bpea)_2](ClO_4)_3$ (1). Single crystals were grown by slow diffusion of hexanes into an acetonitrile–chloroform (1:1) solution of **1**. A crystal of dimensions 0.31 × 0.24 × 0.22 mm was coated with oil (Paratone-N, Exxon Chemical Co.) and mounted on a glass fiber. The crystal was rapidly transferred to a cold stream of nitrogen (202 K). Unit cell parameters were determined by the least-squares fitting of 24 reflections (including Friedel pairs) having 2θ values within 23–25°. The stability of the crystal was monitored by measuring the intensities of three check reflections after every 1 h. No decay was observed in the 34 h of exposure to X-radiation. The ψ-scans[43] of three reflections with θ in the range 5–12° and χ within 81–85° were used for an empirical absorption correction. Compound **1** crystallizes in the triclinic system. The structure was successfully solved in the space group $P\bar{1}$ (No. 2) by direct methods[44] and refined by standard full-matrix least-squares and Fourier techniques on a Digital Equipment MicroVAX computer using locally modified Enraf-Nonius SDP software.[45] Significant crystal information and data collection parameters are summarized in Table I. The asymmetric unit contains one molecule of **1** with one acetonitrile and half of a chloroform molecule.

(38) Sawyer, D. T.; Roberts, J. L. *Experimental Electrochemistry for Chemists*; Wiley: New York, 1974; p 212.
(39) Hatfield, W. E. In *Theory and Applications of Molecular Paramagnetism*; Boudreaux, E. A., Mulay, L. N., Eds.; Wiley: New York, 1976; pp 491–495.
(40) Woodward, W. S.; Rocklin, R. D.; Murray, R. W. *Chem. Biomed. Environ. Instrum.* **1979**, *9*, 95.
(41) Symbols: q, quartet; t, triplet; d, doublet; s, singlet.
(42) Symbols: vs, very strong; s, strong; m, medium; w, weak; sh, shoulder.
(43) North, A. C. T.; Philips, D. C.; Mathews, F. S. *Acta Crystallogr., Sect. A.* **1968**, *24*, 351–359.
(44) Sheldrick, G. M. *SHELXS-86*, a program for X-ray structure determination; University of Gottingen: Gottingen, FRG, 1986.
(45) Frenz, B. A. *Structure Determination Package*; Texas A&M University and Enraf-Nonius: College Station, TX, and The Netherlands, 1985 (as revised by Dr. F. J. Hollander).

Table II. Atomic Coordinates and Isotropic Equivalent Thermal Parameters[a] for $[Mn_2O_2(O_2CCH_3)(bpea)_2]^{3+}$

atom	x	y	z	B (Å²)
Mn1	0.28071 (7)	0.26071 (7)	0.72931 (7)	2.10 (2)
Mn2	0.29991 (7)	0.29778 (7)	0.90722 (7)	2.23 (2)
O1	0.2917 (3)	0.1817 (3)	0.8572 (3)	2.26 (9)
O2	0.2623 (3)	0.3770 (3)	0.7864 (3)	2.46 (9)
O3	0.4308 (3)	0.2619 (3)	0.7055 (3)	2.5 (1)
O4	0.4492 (3)	0.2877 (3)	0.8626 (3)	2.5 (1)
N1	0.2487 (4)	0.3553 (4)	0.5867 (4)	2.2 (1)
N2	0.3065 (4)	0.1432 (4)	0.6500 (4)	2.2 (1)
N3	0.1281 (4)	0.2539 (4)	0.7364 (4)	2.3 (1)
N4	0.3213 (4)	0.2136 (4)	1.0572 (4)	2.6 (1)
N5	0.3216 (4)	0.4209 (4)	0.9654 (4)	2.5 (1)
N6	0.1516 (4)	0.3089 (4)	0.9670 (4)	2.7 (1)
C1	0.3228 (5)	0.4359 (5)	0.5545 (5)	3.4 (2)
C2	0.2925 (6)	0.5251 (6)	0.4633 (6)	4.7 (2)
C3	0.2546 (5)	0.2874 (5)	0.5089 (5)	3.4 (2)
C4	0.2992 (5)	0.1736 (5)	0.5488 (4)	2.4 (1)
C5	0.3284 (5)	0.1007 (5)	0.4859 (5)	3.7 (2)
C6	0.3621 (6)	−0.0035 (5)	0.5282 (6)	4.4 (2)
C7	0.3674 (6)	−0.0345 (5)	0.6329 (6)	4.0 (2)
C8	0.3390 (5)	0.0412 (5)	0.6916 (5)	3.3 (2)
C9	0.1393 (5)	0.4100 (5)	0.6041 (5)	2.8 (2)
C10	0.0747 (5)	0.3328 (5)	0.6715 (4)	2.5 (1)
C11	−0.0325 (5)	0.3406 (6)	0.6723 (5)	3.8 (2)
C12	−0.0837 (5)	0.2670 (6)	0.7408 (6)	4.7 (2)
C13	−0.0274 (5)	0.1846 (6)	0.8065 (5)	3.7 (2)
C14	0.0788 (5)	0.1803 (5)	0.8013 (5)	2.8 (2)
C15	0.4205 (5)	0.1358 (5)	1.0608 (5)	3.4 (2)
C16	0.4333 (6)	0.0564 (6)	1.1614 (6)	4.5 (2)
C17	0.3205 (5)	0.2923 (5)	1.1243 (5)	3.3 (2)
C18	0.3388 (5)	0.3998 (5)	1.0654 (5)	2.6 (1)
C19	0.3675 (5)	0.4759 (5)	1.1097 (5)	3.8 (2)
C20	0.3771 (6)	0.5745 (5)	1.0498 (6)	4.4 (2)
C21	0.3580 (5)	0.5965 (5)	0.9480 (6)	4.0 (2)
C22	0.3313 (5)	0.5184 (5)	0.9069 (5)	3.2 (2)
C23	0.2281 (5)	0.1570 (5)	1.0858 (5)	2.9 (2)
C24	0.1324 (5)	0.2308 (5)	1.0488 (5)	2.8 (1)
C25	0.0321 (5)	0.2210 (6)	1.0900 (5)	3.9 (2)
C26	−0.0497 (5)	0.2935 (6)	1.0485 (5)	4.4 (2)
C27	−0.0298 (5)	0.3747 (6)	0.9669 (5)	4.0 (2)
C28	0.0722 (5)	0.3804 (5)	0.9275 (5)	3.1 (2)
C29	0.4861 (5)	0.2725 (4)	0.7740 (5)	2.3 (1)
C30	0.6006 (5)	0.2680 (5)	0.7474 (5)	3.3 (2)

[a] The thermal parameter given for anisotropically refined atoms is the isotropic equivalent thermal parameter defined as $(4/3)[a^2\beta(1,1) + b^2\beta(2,2) + c^2\beta(3,3) + ab(\cos\gamma)\beta(1,2) + ac(\cos\beta)\beta(1,3) + bc(\cos\alpha)\beta(2,3)]$, where a, b, and c are real cell parameters and $\beta(i,j)$ are anisotropic β's.

The acetonitrile is disordered with the partial occupancy chloroform on the same site. All of the three perchlorate counterions are disordered in the same manner. For each of them a pseudo-3-fold axis passes through the Cl atom and the single fully occupied O atom, while the other three O atoms are disordered among a total of six positions around this 3-fold axis. All non-hydrogen atoms having full occupancies were refined by using anisotropic thermal parameters. Hydrogen atoms were located on difference Fourier map and included in the structure factor calculation at idealized positions, but not refined. Atomic coordinates and equivalent isotropic thermal parameters for the cation are listed in Table II.

B. $[Mn_3O_4(OH)(bpea)_3](ClO_4)_3$ (2). Crystals of **2** suitable for X-ray diffraction experiments were obtained by slow evaporation of an acetonitrile–toluene (2:1) solution. A crystal of dimensions 0.32 × 0.62 × 0.41 mm was taken from the mother liquor, coated with oil (Paratone-N, Exxon Chemical Co.), and transferred to the diffractometer nitrogen cold stream (204 K) after being mounted on a glass fiber. Unit cell parameters were obtained by using a least-squares fit of 24 reflections (including Friedel pairs) having 2θ within the range 24–26°. The space group $P2_1/n$ (No. 14) was uniquely determined from the systematic absences $0k0$, $k = 2n + 1$; $h0l$, $h + l = 2n + 1$. Significant crystal information and data collection parameters are summarized in Table I. Intensities of three check reflections were measured after every hour to monitor the stability of the crystal during data collection. A small intensity reduction (3.7%) was observed in the 58.4 h of exposure to X-radiation. All data were corrected for this decay. An empirical absorption correction was applied based on the ψ-scans[43] of three reflections having θ and χ within 6–15° and 81–84°, respectively. The structure was solved by direct methods and refined as for **1**. The asymmetric unit contains one molecule of **2**. Among the three perchlorate ions, two are disordered in the same fashion: a noncrystallographic 3-fold axis passes through the Cl and O atoms having full occupancy. The other three O atoms are distributed among six sites around this 3-fold axis. The third perchlorate has one O atom in two locations. All non-hydrogen atoms except the partially occupied ones were refined by using anisotropic thermal parameters. Hydrogen atoms of the ligand molecules and that of the hydroxo group were located on a difference Fourier map and included in the structure factor calculation, but not refined. All the hydrogen atoms except that of the hydroxo group were placed at idealized positions. Atomic coordinates and equivalent isotropic thermal param-

Table III. Positional Parameters and Isotropic Equivalent Thermal Parameters[a] for $[Mn_3O_4(OH)(bpea)_3]^{3+}$

atom	x	y	z	B (Å²)
Mn1	0.64584 (8)	0.11793 (3)	0.24049 (5)	2.14 (2)
Mn2	0.79570 (8)	0.19138 (3)	0.30240 (5)	2.16 (2)
Mn3	0.92287 (9)	0.07994 (4)	0.31724 (5)	2.40 (2)
O1	0.6894 (3)	0.1465 (1)	0.3333 (2)	2.17 (9)
O2	0.7205 (4)	0.1726 (1)	0.2085 (2)	2.27 (9)
O3	0.7733 (4)	0.0732 (1)	0.2510 (2)	2.42 (9)
O4	0.9321 (4)	0.1488 (2)	0.3164 (2)	2.59 (9)
O5	0.8612 (4)	0.0714 (2)	0.4006 (2)	2.8 (1)
N1	0.5733 (4)	0.0936 (2)	0.1298 (2)	2.2 (1)
N2	0.5368 (5)	0.0587 (2)	0.2632 (3)	2.5 (1)
N3	0.4702 (4)	0.1548 (2)	0.2185 (3)	2.3 (1)
N4	0.8598 (4)	0.2273 (2)	0.4077 (2)	2.5 (1)
N5	0.6631 (4)	0.2485 (2)	0.2989 (2)	2.3 (1)
N6	0.8981 (5)	0.2481 (2)	0.2701 (2)	2.4 (1)
N7	0.9602 (5)	−0.0009 (2)	0.3231 (3)	2.8 (1)
N8	1.1031 (4)	0.0752 (2)	0.3885 (3)	2.6 (1)
N9	1.0026 (5)	0.0716 (2)	0.2265 (3)	2.8 (1)
C1	0.6762 (6)	0.0880 (2)	0.0893 (3)	2.9 (1)
C2	0.6318 (6)	0.0763 (3)	0.0069 (3)	3.6 (2)
C3	0.5076 (7)	0.0437 (2)	0.1306 (4)	3.5 (2)
C4	0.4827 (6)	0.0298 (2)	0.2043 (3)	2.8 (1)
C5	0.4096 (6)	−0.0117 (3)	0.2133 (4)	3.7 (2)
C6	0.3911 (7)	−0.0233 (3)	0.2812 (4)	4.3 (2)
C7	0.4456 (6)	0.0068 (3)	0.3408 (4)	3.9 (2)
C8	0.5183 (6)	0.0477 (2)	0.3307 (4)	3.3 (2)
C9	0.4853 (6)	0.1354 (2)	0.0941 (3)	3.0 (2)
C10	0.4118 (5)	0.1562 (2)	0.1459 (3)	2.6 (1)
C11	0.2934 (6)	0.1779 (3)	0.1236 (4)	3.5 (2)
C12	0.2366 (6)	0.1989 (3)	0.1743 (4)	4.3 (2)
C13	0.2981 (6)	0.1972 (3)	0.2492 (4)	3.8 (2)
C14	0.4138 (6)	0.1741 (2)	0.2691 (3)	2.9 (1)
C15	0.9423 (7)	0.1918 (3)	0.4634 (3)	3.6 (2)
C16	0.9771 (7)	0.2118 (3)	0.5428 (3)	3.7 (2)
C17	0.7407 (6)	0.2397 (2)	0.4303 (3)	2.8 (1)
C18	0.6476 (6)	0.2630 (2)	0.3658 (3)	2.7 (1)
C19	0.5515 (6)	0.2961 (3)	0.3723 (4)	3.5 (2)
C20	0.4707 (6)	0.3148 (3)	0.3092 (4)	3.6 (2)
C21	0.4894 (6)	0.3009 (2)	0.2411 (4)	3.3 (2)
C22	0.5857 (6)	0.2679 (2)	0.2373 (3)	3.1 (2)
C23	0.9308 (6)	0.2749 (3)	0.3984 (3)	3.4 (2)
C24	0.9549 (6)	0.2817 (2)	0.3232 (3)	2.7 (1)
C25	1.0268 (7)	0.3205 (3)	0.3071 (4)	4.4 (2)
C26	1.0409 (7)	0.3265 (3)	0.2356 (4)	5.2 (2)
C27	0.9789 (7)	0.2931 (3)	0.1806 (4)	4.2 (2)
C28	0.9090 (6)	0.2541 (2)	0.1997 (3)	2.8 (1)
C29	0.8377 (6)	−0.0300 (2)	0.3038 (4)	3.5 (2)
C30	0.8475 (8)	−0.0874 (3)	0.3209 (5)	5.3 (2)
C31	1.0291 (6)	−0.0100 (2)	0.4017 (3)	3.3 (2)
C32	1.1255 (6)	0.0304 (2)	0.4256 (3)	2.8 (1)
C33	1.2325 (7)	0.0242 (3)	0.4831 (4)	3.9 (2)
C34	1.3146 (7)	0.0647 (3)	0.5019 (4)	4.7 (2)
C35	1.2920 (7)	0.1096 (3)	0.4625 (4)	4.3 (2)
C36	1.1833 (6)	0.1139 (3)	0.4061 (3)	3.4 (2)
C37	1.0429 (6)	−0.0143 (3)	0.2728 (4)	3.6 (2)
C38	1.0367 (6)	0.0246 (3)	0.2115 (3)	3.3 (2)
C39	1.0693 (7)	0.0131 (3)	0.1458 (4)	4.5 (2)
C40	1.0658 (7)	0.0509 (3)	0.0940 (4)	4.8 (2)
C41	1.0269 (7)	0.0990 (3)	0.1080 (4)	4.6 (2)
C42	0.9953 (6)	0.1083 (3)	0.1752 (4)	3.6 (2)

[a] The thermal parameter given for anisotropically refined atoms is the isotropic equivalent thermal parameter defined as $(4/3)[a^2\beta(1,1) + b^2\beta(2,2) + c^2\beta(3,3) + ab(\cos\gamma)\beta(1,2) + ac(\cos\beta)\beta(1,3) + bc(\cos\alpha)\beta(2,3)]$, where a, b, and c are real cell parameters and $\beta(i,j)$ are anisotropic β's.

Table IV. Selected Bond Distances[a] and Angles[b] for $[Mn_2O_2(O_2CCH_3)(bpea)_2](ClO_4)_3 \cdot CH_3CN \cdot 0.5CHCl_3$ ($1 \cdot CH_3CN \cdot 0.5CHCl_3$)[c]

Distances								
Mn1	O1	1.799 (4)	Mn1	N2	2.008 (5)	Mn2	O4	1.949 (4)
Mn1	O2	1.808 (4)	Mn1	N3	1.984 (5)	Mn2	N4	2.088 (5)
Mn1	O3	1.936 (4)	Mn2	O1	1.803 (4)	Mn2	N5	1.999 (5)
Mn1	N1	2.074 (5)	Mn2	O2	1.786 (4)	Mn2	N6	1.988 (5)

Angles											
O1	Mn1	O2	87.1 (2)	O3	Mn1	N2	85.3 (2)	O2	Mn2	O4	93.0 (2)
O1	Mn1	O3	92.6 (2)	O3	Mn1	N3	172.6 (2)	O2	Mn2	N4	171.4 (2)
O1	Mn1	N1	173.1 (2)	N1	Mn1	N2	82.8 (2)	O2	Mn2	N5	95.3 (2)
O1	Mn1	N2	99.4 (2)	N1	Mn1	N3	81.2 (2)	O2	Mn2	N6	91.8 (2)
O1	Mn1	N3	92.2 (2)	N2	Mn1	N3	88.4 (2)	O4	Mn2	N4	95.1 (2)
O2	Mn1	O3	91.9 (2)	O1	Mn2	O2	87.6 (2)	O4	Mn2	N5	85.6 (2)
O2	Mn1	N1	91.1 (2)	O1	Mn2	O4	90.3 (2)	O4	Mn2	N6	174.0 (2)
O2	Mn1	N2	173.1 (2)	O1	Mn2	N4	95.0 (2)	N4	Mn2	N5	82.7 (2)
O2	Mn1	N3	94.0 (2)	O1	Mn2	N5	175.1 (2)	N4	Mn2	N6	79.9 (2)
O3	Mn1	N1	94.1 (2)	O1	Mn2	N6	93.5 (2)	N5	Mn2	N6	90.5 (2)
Mn1	O1	Mn2	91.5 (2)	Mn1	O2	Mn2	91.7 (2)				

[a] In angstroms. [b] In degrees. [c] Numbers in parentheses are estimated standard deviations in the least significant digits.

Table V. Selected Structural, Electrochemical, and Magnetic Parameters for Compounds with the $[Mn_2O_2]^{4+}$ Core

compd	Mn–O (Å)	Mn–O–Mn (deg)	Mn–Mn (Å)	$E_{1/2}$ (V)[a]	J (cm^{-1})	ref
$[Mn_2O_2(salpn)_2]$	1.819 (2)	97.2 (1)	2.728 (1)	−0.40	−82	50
$[Mn_2O_2(pic)_2]$	1.819 (3)	98.1 (2)	2.747 (2)	0.66	−87	51
$[Mn_2O_2(bispicen)_2]^{4+}$	1.812 (3)	95.2 (2)	2.676 (2)	1.00	−127	52
$[Mn_2O_2(phen)_2]^{4+}$	1.801 (4)	99.5 (2)	2.748 (2)	1.25	−144	22
$[Mn_2O_2(dmepa)_2]^{4+}$	1.77 (3)	101.5 (2)	2.747 (18)	1.28	−131	53
$[Mn_2O_2(O_2CCH_3)(tpen)]^{3+}$	1.798 (3)	92.2 (2)	2.591 (1)	0.90		54
$[Mn_2O_2(tpma)_2]^{4+}$				1.20	−137	25
$[Mn_2O_2(bispictn)_2]^{4+}$	1.803 (14)	97.8 (4)	2.719 (3)	1.01	−105	55
$[Mn_2O_2(bispicbn)_2]^{4+}$				0.96	−121	55
$[Mn_2O_2(bispichxn)_2]^{4+}$				0.97	−116	55
$[Mn_2O_2(O_2CCH_3)(bpea)_2]^{3+}$	1.799 (4)	91.6 (2)	2.580 (1)	0.93	−124	this work

[a] Potentials for Mn(IV)–Mn(IV)/Mn(IV)–Mn(III) reduction (reference electrode SCE).

eters for the cation are given in Table III.

Results and Discussion

Synthesis. The reaction conditions used to prepare compound **1** were similar to those employed previously[22,46] for $[Mn_2O_2(bpy)_4]^{3+}$. We propose that upon addition of acid the mixed-valence (III,IV) species $[Mn_2O_2(O_2CCH_3)(bpea)_2]^{2+}$ forms initially and then disproportionates to give the IV,IV dimer along with a Mn^{II} species. This hypothesis is supported by two observations: (i) the yield of **1** was low and (ii) the reaction mixture filtrate was quite lightly colored, indicating that the remaining manganese is in a low oxidation state. The disproportionation of binuclear manganese(III,IV) complexes has been observed previously.[37,46] Disproportionation of $Mn^{III,III}{}_2$ species is also known.[7]

Conversion from binuclear to trinuclear bpea species was accomplished in a 1:5 CH_3CN/H_2O mixture with a large excess of perchlorate present. The excess ClO_4^- is required to salt out the trinuclear product. If it is not present, the yield of **2** is greatly decreased and one observes a significant amount of an insoluble dark material, presumably MnO_2. The formation of **2** is nearly quantitative (90% yield) and can be described by eq 1. The stoichiometry shown in eq 1 suggests that one out of every three dimers is cannibalized during the course of the reaction. The

$$3[Mn_2O_2(O_2CCH_3)(bpea)_2]^{3+} + 4H_2O \xrightarrow{H_2O/CH_3CN} 2[Mn_3O_4(OH)(bpea)_3]^{3+} + 3HO_2CCH_3 + 3H^+ \quad (1)$$

synthesis of **4** as described by Sarneski et al.[37] involves a similar binuclear to trinuclear conversion process in aqueous nitric acid. Although compound **4** is an $Mn^{IV}{}_3$ species, the starting material used in its synthesis is the well-known mixed-valence (III,IV) complex $[Mn_2O_2(bpy)_4]^{3+}$. It was assumed that a disproportionation reaction takes place in acidic medium, affording 1 equiv of Mn^{2+} for each equivalent of **4** produced.[37] In contrast, our synthesis of **2** employes a $Mn^{IV,IV}{}_2$ starting material, thus being more efficient on a per manganese basis.

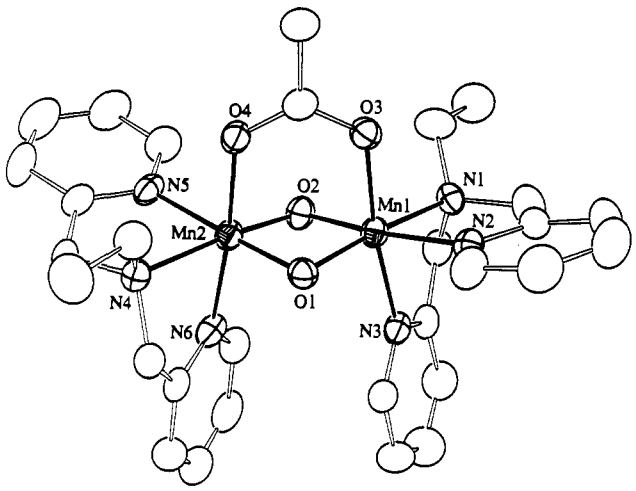

Figure 2. Structure of $[Mn_2O_2(O_2CCH_3)(bpea)_2]^{3+}$ (**1**) showing the 50% probability thermal ellipsoids and atom-labeling scheme. Hydrogen atoms are omitted.

Structures. The crystal structure of **1**, shown in Figure 2, is the first example of a species containing a $\{Mn^{IV}{}_2(\mu\text{-}O)_2(O_2CCH_3)\}^{3+}$ core. The one-electron-reduced core $\{Mn^{III,IV}{}_2O_2(O_2CCH_3)\}^{2+}$ has been observed previously.[47-49] Also, there are a growing number of structurally characterized complexes containing the $\{Mn^{IV}{}_2(\mu\text{-}O)_2\}^{4+}$ core that lack the bridging acetate moiety.[20,22,25,50-55] Selected bond distances and angles for **1** are

(46) Cooper, S. R.; Calvin, M. *J. Am. Chem. Soc.* **1977**, *99*, 6623–6630.
(47) Wieghardt, K.; Bossek, U.; Zsolnai, L.; Huttner, G.; Blondin, G.; Girerd, J.-J.; Babonneau, F. *J. Chem. Soc., Chem. Commun.* **1987**, 651–653.
(48) Bashkin, J. S.; Schake, A. R.; Vincent, J. B.; Chang, H.-R.; Li, Q.; Huffman, J. C.; Christou, G.; Hendrickson, D. N. *J. Chem. Soc., Chem. Commun.* **1988**, 700–702.
(49) Pal, S.; Gohdes, J. W.; Wilisch, W. C. A.; Armstrong, W. H. *Inorg. Chem.* **1992**, *31*, 713–716.

Table VI. Selected Bond Distances[a] and Angles[b] for $[Mn_3O_4(OH)(bpea)_3](ClO_4)_3$ (**2**)[c]

			Distances					
Mn1	O1	1.822 (4)	Mn2	O1	1.828 (4)	Mn3	O3	1.795 (3)
Mn1	O2	1.807 (4)	Mn2	O2	1.797 (3)	Mn3	O4	1.799 (4)
Mn1	O3	1.786 (4)	Mn2	O4	1.821 (4)	Mn3	O5	1.830 (4)
Mn1	N1	2.103 (4)	Mn2	N4	2.118 (4)	Mn3	N7	2.145 (5)
Mn1	N2	2.050 (5)	Mn2	N5	2.064 (5)	Mn3	N8	2.087 (4)
Mn1	N3	2.090 (5)	Mn2	N6	2.025 (5)	Mn3	N9	2.072 (5)
O1	H0	2.024 (3)	O5	H0	0.922 (4)			

			Angles							
O1	Mn1	O2	87.0 (2)	O2	Mn2	N4	167.9 (2)	N7	Mn3	N8	76.8 (2)
O1	Mn1	O3	98.3 (2)	O2	Mn2	N5	90.7 (2)	N7	Mn3	N9	80.1 (2)
O1	Mn1	N1	171.1 (2)	O2	Mn2	N6	94.1 (2)	N8	Mn3	N9	89.5 (2)
O1	Mn1	N2	98.6 (2)	O4	Mn2	N4	93.5 (2)	O3	Mn3	O4	97.8 (2)
O1	Mn1	N3	90.8 (2)	O4	Mn2	N5	169.7 (2)	O3	Mn3	O5	96.1 (2)
O2	Mn1	O3	98.8 (2)	O4	Mn2	N6	90.0 (2)	O3	Mn3	N7	93.9 (2)
O2	Mn1	N1	90.9 (2)	N4	Mn2	N5	77.5 (2)	O3	Mn3	N8	170.2 (2)
O2	Mn1	N2	170.9 (2)	N4	Mn2	N6	82.1 (2)	O3	Mn3	N9	85.7 (2)
O2	Mn1	N3	92.0 (2)	N5	Mn2	N6	83.8 (2)	O4	Mn3	O5	99.3 (2)
O3	Mn1	N1	90.6 (2)	O2	Mn2	O4	98.0 (2)	O4	Mn3	N7	166.3 (2)
O3	Mn1	N2	87.6 (2)	O1	Mn2	O2	87.1 (2)	O4	Mn3	N8	91.1 (2)
O3	Mn1	N3	166.2 (2)	O1	Mn2	O4	96.9 (2)	O4	Mn3	N9	93.6 (2)
N1	Mn1	N2	82.5 (2)	O1	Mn2	N4	95.3 (2)	O5	Mn3	N7	86.6 (2)
N1	Mn1	N3	80.6 (2)	O1	Mn2	N5	89.0 (2)	O5	Mn3	N8	86.6 (2)
N2	Mn1	N3	80.8 (2)	O1	Mn2	N6	172.7 (2)	O5	Mn3	N9	166.6 (2)
Mn1	O1	Mn2	90.7 (2)	Mn1	O2	Mn2	92.2 (2)	Mn1	O3	Mn3	124.3 (2)
Mn2	O4	Mn3	124.4 (2)	Mn3	O5	HO	111.7 (3)	O1	HO	O5	138.9 (3)

[a] In angstroms. [b] In degrees. [c] Numbers in parentheses are estimated standard deviations in the least significant digits.

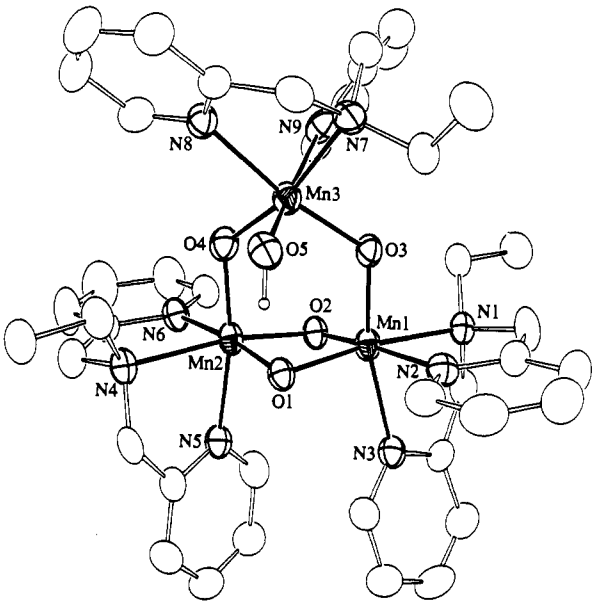

Figure 3. Structure of $[Mn_3O_4(OH)(bpea)_3]^{3+}$ (**2**) depicting the 50% probability thermal ellipsoids and atom-labeling scheme. Hydrogen atoms, except that bound to O5, are omitted for clarity.

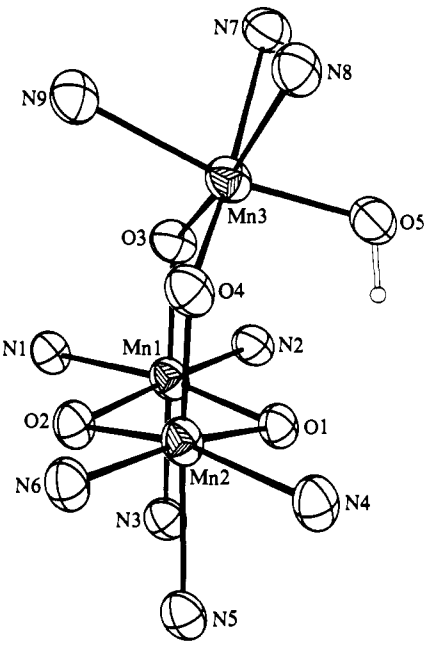

Figure 4. Side-on view of **2** with only the atoms directly coordinated to Mn atoms shown (with the exception of the H atom bound to O5).

listed in Table IV. Inspection of Table V reveals that the Mn–O_{oxo} bond distances in **1** are comparable to those in other di-oxo-bridged Mn^{IV} dimers. A listing of intramolecular Mn···Mn distances and Mn–O–Mn angles for the Mn^{IV}_2 species is also provided in Table V. The bpea ligands in **1** adopt a binding mode that confers pseudo-C_2 symmetry on the complex with, in each case, an aliphatic and an aromatic nitrogen atom trans to bridging oxo groups and the second pyridine nitrogen atoms trans to an acetate oxygen atom. Terminal Mn–O and Mn–N bond distances and angles are unexceptional and are provided in Table IV.

Two views of $[Mn_3O_4(OH)(bpea)_3]^{4+}$ (**2**) are provided in Figures 3 and 4. Bond distances for **2** (Table VI) confirm the oxidation-state assignment Mn^{IV}_3. While at first glance the $\{Mn_3O_4\}^{4+}$ core in **2** resembles that of compounds **3**[36] and **4**,[37] there are several rather distinct differences. Core bond distances and angles for the three trinuclear species are given in Figure 5. Compound **2** possesses a terminally coordinated hydroxo group bound to the apical manganese atom (Mn_a, Figure 1) (Mn–OH, 1.830 (4) Å). This is only the third structurally characterized example of such a Mn–OH moiety, with the previous ones being $[Mn^{III}(5\text{-}NO_2\text{-}sadpen)(OH)]$ (Mn–OH, 1.827 (3) Å)[56] and

(50) (a) Gohdes, J. W.; Armstrong, W. H. *Inorg. Chem.* **1992**, *31*, 368–373. (b) Gohdes, J. W. Ph.D. Dissertation, University of California, Berkeley, 1991.
(51) Libby, E.; Webb, R. J.; Streib, W. E.; Folting, K.; Huffman, J. C.; Hendrickson, D. N.; Christou, G. *Inorg. Chem.* **1989**, *28*, 4037–4040.
(52) Goodson, P. A.; Glerup, J.; Hodgson, D. J.; Michelsen, K.; Pedersen, E. *Inorg. Chem.* **1990**, *29*, 503–508.
(53) Oki, A. R.; Glerup, J.; Hodgson, D. J. *Inorg. Chem.* **1990**, *29*, 2435–2441.
(54) Pal, S.; Armstrong, W. H. To be submitted for publication.
(55) Goodson, P. A.; Glerup, J.; Hodgson, D. J.; Michelsen, K.; Weihe, H. *Inorg. Chem.* **1991**, *30*, 4909–4914.
(56) Eichhorn, D. M.; Armstrong, W. H. *J. Chem. Soc., Chem. Commun.* **1992**, 85–87.

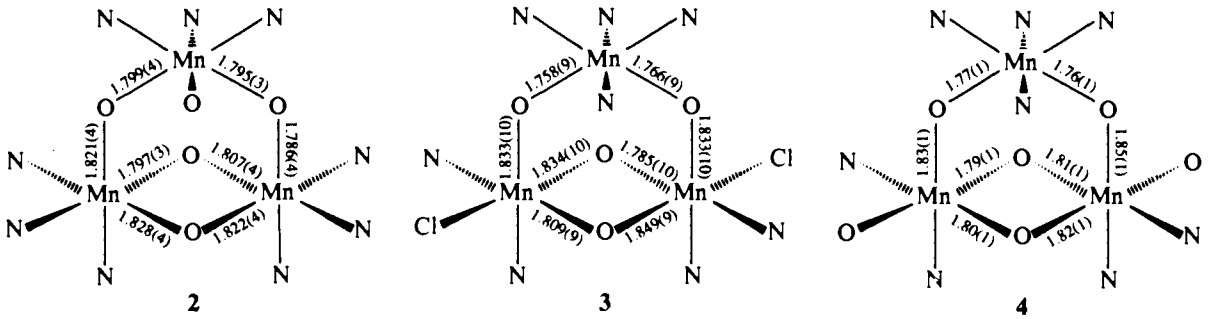

Figure 5. Comparison of the oxo-bridged core structural parameters for the three species that contain the $\{Mn_3O_4\}^{4+}$ unit.

$[Mn^{IV}_2O_2(OH)_2(tacn)_2]^{2+}$ (Mn–OH, 1.881 Å).[57] The proton bound to O5, which was located on a Fourier difference map, is directed toward O1, and the O1···O5 distance (2.786 (5) Å) is consistent with a hydrogen-bonding interaction. This hydrogen bond appears to be responsible in part for a distortion of the core such that Mn3 is "pulled" toward O1, resulting in a dihedral angle between the planes defined by Mn1, Mn2, O3, and O4 and Mn3, O3, and O4 of 26.6°. In contrast, the corresponding dihedral angles in **3** and **4** are 0°. The *average* $Mn–O_{oxo}$ distance in the basal Mn_2O_2 plane of **2** is very close to values observed for **3**[36] and **4**.[37] However, it is interesting to note that for **2** the Mn–O distances to O1 are distinctly longer (1.828 (4), 1.822 (4) Å) than the distances to O2 (1.797 (3), 1.807 (4) Å). This could be a consequence of the internal hydrogen-bonding interaction somewhat weakening the π bonds to O1. *Average* $Mn–O_a$ bond lengths in all three trinuclear species are almost identical; however, the pattern of the distribution of distances in **2** is different and worth noting. For **3** and **4**, $Mn_b–O_a$ (Figure 1) distances are distinctly longer than $Mn_a–O_a$ distances. On the other hand, although compound **2** has about the same average $Mn–O_a$ bond length, the distinction between $Mn_a–O_a$ and $Mn_b–O_a$ distances are not as clear-cut as they are for **3** and **4**. The relationship between core structural parameters and magnetic properties is discussed below. Finally, a comparison of Figures 2 and 3 illustrates that the bpea ligand stereochemistry in binuclear **1** is the same as in the basal portion of trinuclear **2**. We have no evidence that other stereoisomers are present in bulk samples of either complex.

Infrared Spectra. The carboxylate O–C–O asymmetric and symmetric vibrations are located at 1560 and 1387 cm^{-1}, respectively for **1**. These values are comparable to those reported for $[Mn_2O_2(O_2CCH_3)(tacn)_2]^{2+}$[47] and $[Mn_2O_2(O_2CCH_3)(tpen)]^{2+}$.[49] Infrared spectroscopy can be used to distinguish **1** and **2**. Obviously, compound **2** lacks the carboxylate-related vibrations. There is also a difference between the spectra in the $Mn–O_{oxo}$ stretching region. As is typical for compounds that contain the $\{Mn_2O_2\}$ core, **1** has a sharp absorption at 669 cm^{-1}. In contrast, the IR spectrum of **2** has a much broader, strong peak centered at 672 cm^{-1}. Presumably this latter absorption corresponds to a vibration related to the basal $\{Mn_2(\mu\text{-}O)_2\}$ portion of **2**, although this may be coupled to $Mn_a–O_a–Mn_b$ vibrations. A distinct $Mn_a–O_a–Mn_b$ asymmetric vibration, such as that observed for $[Mn_4O_6(tacn)_4]^{4+}$[58] and $[Mn_2O(O_2CCH_3)_2L_2]^{n+}$ (L = $HBpz_3$,[29] tacn[28]), is not apparent in the spectrum of **2**.

Electrochemistry. Cyclic voltammetry is another technique that can be used to distinguish compounds **1** and **2** from each other and from other manganese–oxo species. Figure 6 displays the cyclic voltammograms of **1** and **2** in CH_3CN solution at room temperature using a platinum electrode and tetraethylammonium perchlorate (TEAP) as supporting electrolyte. The CV of compound **1** is quite similar to that of other $\{Mn_2O_2\}^{2+/3+/4+}$ species. Two quasireversible reduction processes are evident, with the waves centered at $E_{1/2}$ = +0.93 V (ΔE_p = 60 mV) and $E_{1/2}$ = +0.03 V (ΔE_p = 80 mV) corresponding to the IV,IV/III,IV couple and

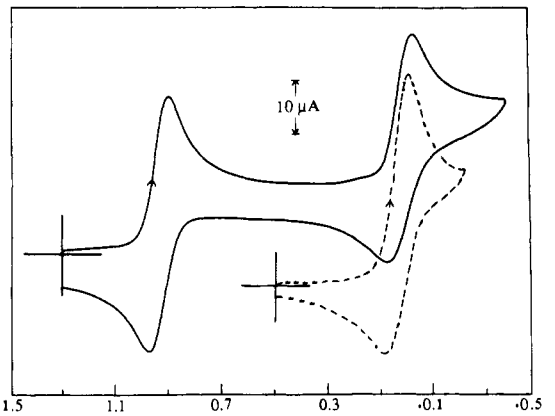

Figure 6. Cyclic voltammograms for **1** (solid line) and **2** (dashed line) in CH_3CN using the experimental conditions described in the text.

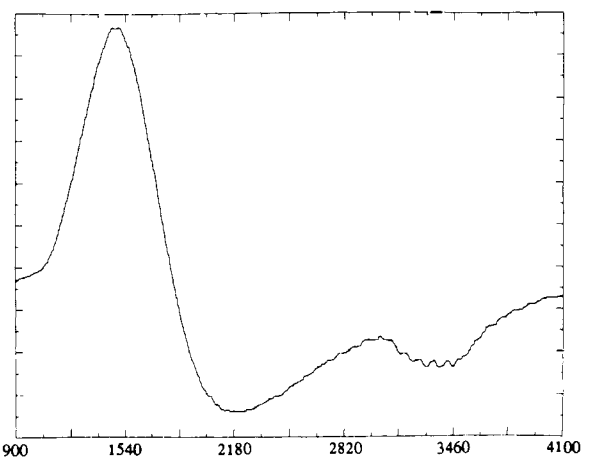

Figure 7. X-band EPR spectrum of **2** in frozen $CH_3CN–C_6H_5CH_3$ (3:1) using the experimental conditions described in the text.

III,IV/III,III couple, respectively. These values may be compared to potentials measured for other $\{Mn_2O_2\}$ species with predominantly nitrogen atom terminal donors (Table V). The first reduction waves fall between 1.28 and 0.90 V vs SCE. Ligands that are much more effective at stabilizing the IV,IV oxidation level, such as the phenolate donors in $[Mn_2O_2(salpn)_2]$, cause a dramatic shift in IV,IV/IV,III potential to –0.40 V vs SCE.[50] Compound **2** has its first reduction at +0.05 V (ΔE_p = 80 mV). Preliminary characterization of derivatives of **2** indicates that this reduction corresponds to the IV/III couple for apical manganese atom Mn_a.[59] Reduction of the basal $\{Mn_2O_2\}$ unit thus occurs at more negative potential, again illustrating the stabilizing influence of the O_a

(57) Wieghardt, K.; Bossek, U.; Nuber, B.; Weiss, J.; Bonvoisin, J.; Corbella, M.; Vitols, S. E.; Girerd, J.-J. *J. Am. Chem. Soc.* **1988**, *110*, 7398–7411.
(58) Wieghardt, K.; Bossek, U.; Gebert, W. *Angew. Chem., Int. Ed. Engl.* **1983**, *22*, 328–329.
(59) Derivatives of **2** wherein the OH^- group is replaced with H_2O, Cl^-, SCN^-, and F^- have been prepared recently in our laboratory. Characterization of these species will be reported elsewhere.

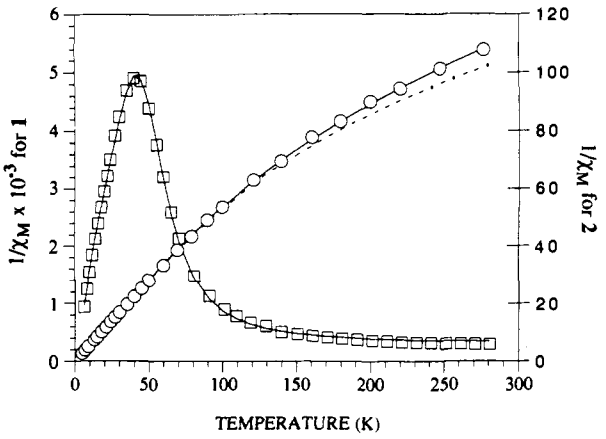

Figure 8. Inverse molar magnetic susceptibility per complex as a function of temperature for **1** (□) and **2** (○). The solid lines were generated from the best fit parameters given in the text. The dashed line represents a theoretical prediction for a simple model ($J' = 0$, Figure 1) for the trinuclear complex **2** (see text).

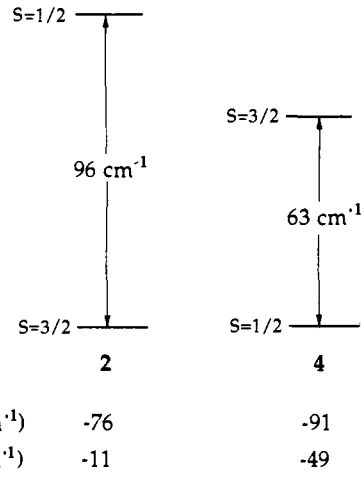

Figure 9. State splitting diagrams and best fit parameters for $[Mn_3O_4(OH)(bpea)_3](ClO_4)_3$ (**2**) and $[Mn_3O_4(H_2O)_2(bpy)_4](ClO_4)_4$ (**4**).[37] Only the first two spin states for each complex are shown.

atoms. The CV scan for **2** is terminated at −0.20 V in Figure 6. If the scan is extended to −1.2 V, a broad irreversible reduction at −0.88 V is observed (not shown).

EPR and Magnetic Properties. Considering the relatively minor structural perturbation in **2** compared to **3** and **4** described above, it was anticipated that **2** would have the same spin ground state ($S = {}^1/_2$) and a similar EPR spectrum with 35 hyperfine lines. To the contrary, the X-band EPR spectrum of **2** at 6 K, shown in Figure 7, is characteristic of a nearly axial $S = {}^3/_2$ state, with a base-line crossing point for the low-field resonance of $g = 3.6$ and a minimum at higher field of $g = 1.92$. The hyperfine lines apparent in the $g = 2$ region of Figure 7 are not associated with $[Mn_3O_4(OH)(bpea)_3]^{3+}$, but rather a small amount of the $Mn^{III,IV}_2$ impurity $[Mn_2O_2(O_2CCH_3)(bpea)_2]^{2+}$ (**5**). The latter complex has been prepared in pure form and characterized by EPR spectroscopy.[60] Splittings in the $g = 2$ region impurity signal match those of **5**. The line shape in Figure 7 is consistent with an axial zero field splitting parameter (D) that is large with respect to the microwave photon energy ($2D \gg h\nu \approx 0.3$ cm^{-1} for X-band frequencies).[61,62]

In order to learn more about the electronic structure of **2** and to confirm the $S = {}^3/_2$ ground-state assignment, variable temperature magnetic susceptibility measurements were carried out. The binuclear precursor **1** was also examined. Inverse susceptibility data for **1** and **2** are provided in Figure 8. The magnetic moment of **1** decreases from 2.78 μ_B at 281 K to 0.22 μ_B at 6 K. The data for **1** were fit using the standard isotropic spin Hamiltonian $\mathcal{H} = -2J\hat{S}_1\cdot\hat{S}_2$, where $S_1 = S_2 = {}^3/_2$.[63] Addition of an impurity term was required in order to achieve a satisfactory fit. The parameters used to obtain the theoretical fit shown in Figure 9 are $J = -124$ (1) cm^{-1}, $g = 2.29$ (3), and $p = 0.14\%$. The exchange parameter J determined for **1** is comparable to that determined for other IV,IV dimers with nitrogen atom terminal ligation (Table V) and significantly higher than J values reported for $[Mn_2O_2(salpn)_2]$ (**6**) ($J = -82$ cm^{-1})[50] and $[Mn_2O_2(pic)_4]$ (**7**) ($J = -87$ cm^{-1}).[51] The smaller J parameters for **6** and **7** are important with regard to the comparable value determined for the basal $\{Mn_2O_2\}$ unit of **2** (see below).

As shown in Table V, the magnetic exchange parameter J has been determined for a total of seven structurally characterized species that contain the $\{Mn_2O_2\}^{4+}$ core. It has been suggested that in these compounds magnetic exchange is dominated by direct d_{xy}–d_{xy} orbital overlap, where the x and y axes are coincident with Mn–(μ-O) bonds.[9] If this were correct, a strong correlation between Mn···Mn distance and J would be expected. While there is a good correlation between these parameters when all oxidation states of the $\{Mn_2O_2\}^{n+}$ core are considered ($n = 2, 3, 4$) along with species that have other core types ($\{Mn_2O(O_2CCH_3)_2\}$ and $\{Mn_2O_3\}$),[9] if one examines only the set of $\{Mn_2O_2\}^{4+}$ compounds (Table V), the correlation is poor. Consider, for example, the fact that $[Mn_2O_2(phen)_4]^{4+}$ has one of the *longest* Mn···Mn distances (2.747 (2) Å) yet the *strongest* antiferromagnetic exchange ($J = -144$ cm^{-1}).[22] Furthermore, the picolinate dimer $[Mn_2O_2(pic)_4]$ has virtually the same Mn···Mn distance (2.747 Å) as the phen species; however, its antiferromagnetic exchange is among the weakest ($J = -87$ cm^{-1}).[51] This does not rule out a contribution to antiferromagnetic exchange from direct overlap, however, in our opinion one cannot make a strong case that it is the dominating contribution.[64]

That **2** behaves as an $S = {}^3/_2$ paramagnet is readily apparent from Figure 8; the linear region in $1/\chi_m$ at low temperature (slope = 0.54 emu K/mol) confirms this conclusion. The magnetic moment of **2** is 4.53 μ_B at 277 K and decreases to a value consistent with an $S = {}^3/_2$ spin state, 3.77 μ_B, at 5 K. The dashed line shown in Figure 8 corresponds to simply adding the data for the Mn^{IV}_2 dimer **1** to a contribution from a mononuclear Mn^{IV} center (see Table S9). This simple model corresponds to a trinuclear species for which the "basal" magnetic interaction J remains unchanged and the apical interactions J' (Figure 1) are equal to 0. This $J' = 0$ model deviates from the data significantly at high temperature. Thus we chose to fit the data for **2** using a two-J treatment (Figure 1) as was done for **3**[36] and **4**[37] previously. The Hamiltonian employed is given in eq 2. The fit shown in Figure 8 was obtained

$$\mathcal{H} = -2J(\hat{S}_1\cdot\hat{S}_2) - 2J'(\hat{S}_1\cdot\hat{S}_3 + \hat{S}_2\cdot\hat{S}_3) \qquad (2)$$

using the following parameters: $J = -76$ (1) cm^{-1}, $J' = -11$ (1) cm^{-1}, and $g = 1.964$ (7). Since an excellent fit was obtained using these parameters, we did not adjust the theoretical model to include zero field splitting (D). In order to determine the magnitude of D to a high degree of precision, variable field measurements at low temperatures will be carried out in the future. The magnetic susceptibility best fit parameters for the two other $\{Mn_3O_4\}^{4+}$ core complexes are as follows: **3**, $J = -85$ cm^{-1}, $J' = -54$ cm^{-1}; **4**, $J = -91$ cm^{-1}, $J' = -49$ cm^{-1}. The smaller basal J value for **2** as compared to **1** and other binuclear (IV,IV) species may be in part a consequence of the longer average Mn_b–O_b distances for the former. The oxo superexchange pathway is probably strongly affected by changes in the Mn–O_{oxo} bond distances. This point was raised previously for $\{Mn_2O_2\}^{4+}$ dimers,[50] and a strong correlation between Fe–O_{oxo} bond distances and magnetic exchange values in $\{Fe_2O\}^{4+}$ complexes has been observed.[65] The average

(60) Pal, S.; Armstrong, W. H. Unpublished results.
(61) Pedersen, E.; Toftlund, H. *Inorg. Chem.* **1974**, *13*, 1603–1612.
(62) Hempel, J. C.; Morgan, L. O.; Lewis, W. B. *Inorg. Chem.* **1970**, *9*, 2064–2072.
(63) O'Connor, C. J. *Prog. Inorg. Chem.* **1982**, *29*, 204–283.

(64) The issue of direct metal–metal interaction in $\{Mn_2O_2\}^{4+}$ cores is also discussed in ref 50b. Further analysis of the arguments put forth in ref 9 will appear elsewhere: Armstrong, W. H.; Pal, S. *Chem. Rev.*, to be submitted.

Mn_b–O_b distance in **2** (1.814 Å) is very close to that for $[Mn_2O_2(salpn)_2]$ (1.819 Å) and is significantly longer than Mn–O_{oxo} distances in compounds that have substantially larger J values (Table V). The most dramatic difference between the magnetic parameters of **2** and the bpy trinuclear species lies in their J' values. The relationship between J' and structure and how this relates to ground spin state variability are dealt with in the next section.

Ground Spin State Variability. The principal origin of the spin-state change in going from **3** and **4** ($S = {}^1/_2$) to **2** ($S = {}^3/_2$) appears to be the magnitude of J', which is approximately 5-fold smaller in the latter. The structural change that is most likely responsible for a decrease in J' is the "pulling" of Mn_a toward O1, shown clearly in Figure 4. Presumably the hydrogen bonding between O1 and O5 is at least partially responsible for this distortion. Of course, steric factors may contribute as well. For **3** and **4**, both sides of the $(Mn_b)_2(O_a)_2$ plane (Figure 1) are equivalent; thus Mn_a resides in that plane, and any intramolecular steric interactions are counterbalanced. For **2**, on the other hand, both sides of the $(Mn_b)_2(O_a)_2$ plane are not equivalent, by virtue of a single OH group on one side and also the fact that bpea binds unsymmetrically with respect to that plane.

The separations between lowest lying $S = {}^3/_2$ and $S = {}^1/_2$ states for **2** and **4** are illustrated in Figure 9. The J'/J ratio determines which state is the ground state. When $J'/J \approx 0.4$, the $S = {}^1/_2$ and $S = {}^3/_2$ states are degenerate. For **4**, where $J'/J = 0.54$, the ground state is $S = {}^1/_2$ and the $S = {}^3/_2$ state is 63 cm^{-1} higher in energy. However for **2**, J'/J (0.14) lies on the other side of the crossing point because J' is so much smaller than for **3** and **4**. Consequently, the $S = {}^3/_2$ state is the ground state in **2** and the $S = {}^1/_2$ state lies 96 cm^{-1} higher, as shown in Figure 9.

There are at least two readily apparent explanations for the decrease in J' observed for **2** with respect to **3** and **4**: (i) the extent of orbital overlaps which correspond to dominant superexchange pathway(s) between basal and apical manganese atoms (Figure 1) is markedly angle-dependent, and (ii) the hydroxide donor to Mn_a alters the $d\pi$ orbital energies to such a degree that superexchange orbital overlap is diminished. At this point we favor explanation i as the dominating influence, although in order to confirm this we must examine species for which OH^- has been replaced with H_2O and Cl^-, for example.[59]

Ground spin state changes for other polynuclear iron and manganese oxo species at a given overall oxidation state have been observed previously. As stated above, compounds with the $\{Mn_2O(O_2CCH_3)_2\}^{2+}$ core structure can have either $S = 0$ (low spin) or $S = 4$ (high spin) ground states.[27-29] We have shown[66] that the adamantane-shaped $\{Mn_4O_6\}^{4+}$ core can be high spin or low spin, depending on its protonation state. Finally, the equilateral triangular $\{Fe_3O\}^{7+}$ core exhibits an $S = {}^1/_2$ ground state, whereas Gorun and Lippard have demonstrated[67] that an isosceles or "t-shaped" $\{Fe_3O\}^{7+}$ species has an $S = {}^5/_2$ ground state.

Concluding Remarks. We have demonstrated the existence of an $\{Mn_3O_4\}^{4+}$ core type that possesses an $S = {}^3/_2$ ground state in distinct contrast to results for other such species. The principal structural distortion responsible for the electronic structural change has been identified and seems to be more easily recognizable than in the $\{Fe_4S_4\}^+$ case. When taken together, trinuclear complexes $[Mn_3O_4(OH)(bpea)_3]^{3+}$, $[Mn_3O_4Cl_2(bpy)_4]^{2+}$, and $[Mn_3O_4(OH_2)_2(bpy)_4]^{4+}$ demonstrate the existence of ground spin state ${}^1/_2 \leftrightarrow {}^3/_2$ variability in polynuclear manganese oxo chemistry. This provides us with a clue as to how similar structural changes in the MnOEC may give rise to ${}^1/_2 \leftrightarrow \geq {}^3/_2$ ground spin state changes therein.

Acknowledgment. Funding for this work was provided by Grant No. GM382751 from the National Institute of General Medical Sciences. We thank Melissa Grush for assistance with recording the EPR spectrum (Figure 7) and Dr. Joel W. Gohdes for supplying the magnetic data.

Supplementary Material Available: Fully labeled ORTEP drawings (Figures S1 and S2), atomic positional parameters (Tables S1 and S5), anisotropic thermal parameters (Tables S2 and S6), intramolecular bond distances (Tables S3 and S7), and intramolecular bond angles (Tables S4 and S8) for **1**·CH_3CN·$0.5CHCl_3$ and **2**, and experimental and calculated inverse molar susceptibilities as a function of temperature for **1** and **2** (Table S9) (18 pages); observed and calculated structure factors for **1**·CH_3CN·$0.5CHCl_3$ and **2** (72 pages). Ordering information is given on any current masthead page.

(65) Gorun, S. M.; Lippard, S. J. *Inorg. Chem.* **1991**, *30*, 1625–1630.

(66) Hagen, K. S.; Westmoreland, T. D.; Scott, M. J.; Armstrong, W. H. *J. Am. Chem. Soc.* **1989**, *111*, 1907–1909.

(67) Gorun, S. M.; Lippard, S. J. *J. Am. Chem. Soc.* **1985**, *107*, 4568–4570.